Materials Today Bio 15 (2022) 100323

Contents lists available at ScienceDirect

Materials Today Bio

journal homepage: www.journals.elsevier.com/materials-today-bio

Molecular stiffness cues of an interpenetrating network hydrogel for cell adhesion

Bin Li [a,*,1], Arzu Çolak [a,1], Johanna Blass [a], Mitchell Han [a], Jingnan Zhang [a,b], Yijun Zheng [a], Qiyang Jiang [a,b], Roland Bennewitz [a,c,**], Aránzazu del Campo [a,b,***]

[a] INM–Leibniz Institute for New Materials Campus D2 2, 66123, Saarbrücken, Germany
[b] Chemistry Department, Saarland University, 66123, Saarbrücken, Germany
[c] Physics Department, Saarland University, 66123, Saarbrücken, Germany

ARTICLE INFO

Keywords:
IPNs
Nanomechanics
Mechanotransduction
Cell adhesion
AFM

ABSTRACT

Understanding cells' response to the macroscopic and nanoscale properties of biomaterials requires studies in model systems with the possibility to tailor their mechanical properties and different length scales. Here, we describe an interpenetrating network (IPN) design based on a stiff PEGDA host network interlaced within a soft 4-arm PEG-Maleimide/thiol (guest) network. We quantify the nano- and bulk mechanical behavior of the IPN and the single network hydrogels by single-molecule force spectroscopy and rheological measurements. The IPN presents different mechanical cues at the molecular scale, depending on which network is linked to the probe, but the same mechanical properties at the macroscopic length scale as the individual host network. Cells attached to the interpenetrating (guest) network of the IPN or to the single network (SN) PEGDA hydrogel modified with RGD adhesive ligands showed comparable attachment and spreading areas, but cells attached to the guest network of the IPN, with lower molecular stiffness, showed a larger number and size of focal adhesion complexes and a higher concentration of the Hippo pathway effector Yes-associated protein (YAP) than cells linked to the PEGDA single network. The observations indicate that cell adhesion to the IPN hydrogel through the network with lower molecular stiffness proceeds effectively as if a higher ligand density is offered. We claim that IPNs can be used to decipher how changes in ECM design and connectivity at the local scale affect the fate of cells cultured on biomaterials.

Cells sense and respond to the mechanical and biochemical properties of the extracellular matrix (ECM), i.e., the hydrogel network to which they are connected [1,2]. Studies performed in model matrices with defined biochemical and mechanical cues have provided fundamental knowledge on mechanosensing and mechanotransduction mechanisms and length scales by offering experimentally simplified contexts that facilitate parametric analysis and quantification [3–5]. One open front of debate is the importance of nanoscale mechanics in regulating cell behavior [6], which has been supported by recent experimental evidence using biomaterials modified by cell adhesive ligands linked with spacers of different lengths, or protein nanosheets at liquid-liquid interfaces with different shear stress moduli [7–9]. These results raise the question of how to include nanomechanical cues in experimental models well-established in cell mechanobiology research [10], i.e., in synthetic hydrogels with tailored bulk mechanical properties, like stiffness or stress relaxation, measured by rheology or indentation with colloidal probes.

The natural ECM can be understood as an interpenetrating polymer network of structural molecules that interact in a number of ways to form interconnected architectures. The IPN structure provides flexibility for remodeling of the individual networks without compromising the integrity of the tissue, offering multiple possibilities to encode mechanical information. This can also be observed in synthetic materials. For example, using an IPN design, a covalently crosslinked poly (acrylamide) (PAAm) network interpenetrated by linear high-molecular-weight PAAm chains was used to study cell responses to changes in bulk elasticity and viscoelastic dissipation, which were tuned independently by the ratio of

* Corresponding author. Physical Department E22, Technical University of Munich, 85748, Garching, Germany.
** Corresponding author. INM–Leibniz Institute for New Materials Campus D2 2, 66123, Saarbrücken, Germany.
*** Corresponding author. INM–Leibniz Institute for New Materials Campus D2 2, 66123, Saarbrücken, Germany.
E-mail addresses: bin1.li@tum.de (B. Li), roland.bennewitz@leibniz-inm.de (R. Bennewitz), aranzazu.delcampo@leibniz-inm.de (A. Campo).
[1] Dr. B. Li and Dr. A. Çolak contributed equally.

https://doi.org/10.1016/j.mtbio.2022.100323
Received 22 January 2022; Received in revised form 24 May 2022; Accepted 9 June 2022
Available online 17 June 2022

the two networks [11].

We propose here IPN hydrogels that present the same mechanical properties at the macroscale but encode different mechanical responses at the molecular scale within a single macroscopic material, and we study the ability of cells to sense them. The hydrogel is an IPN with two individual PEG networks which are interpenetrated but not covalently linked to each other, since they were prepared in two steps and crosslinked via orthogonal reactions. The two individual networks can be modified with bioactive ligands independently and at desired ligand density. Atomic Force Microscopy (AFM) with single-bond sensitivity is used to quantify the local mechanics of the two individual networks within the IPN the SN, in an attempt to compare the mechanical responses at molecular, i.e. single cell receptor scale. Cell response at the level of cell density, spreading area, focal adhesion formation and YAP distribution in cells attached by cell adhesive ligands linked to individual networks of the IPN or to the SN is quantified. The obtained results are discussed in terms of differences in molecular flexibility and effective higher linker density in the softer local environment.

Single network and interpenetrating network hydrogel films (Fig. 1a) were synthesized starting from poly (ethylene glycol) (PEG) precursors in a two-step process. The SN (host network) was prepared by photo-initiated copolymerization of PEG-diacrylate (PEGDA) macromonomer and carboxy PEG acrylate (ACPEG-COOH) (Fig. 1b). The polymerization time was extracted from rheological studies of the photopolymerization kinetics (Figure S4b). PEGDA/COOH gels with Young's Modulus of 40 kPa were obtained from 15% to 3% (*w/v*) mixtures of PEGDA and ACPEG comonomers, respectively. Hydrogel films with a swollen thickness around 140 μm were prepared (Figure S1 in SI)..

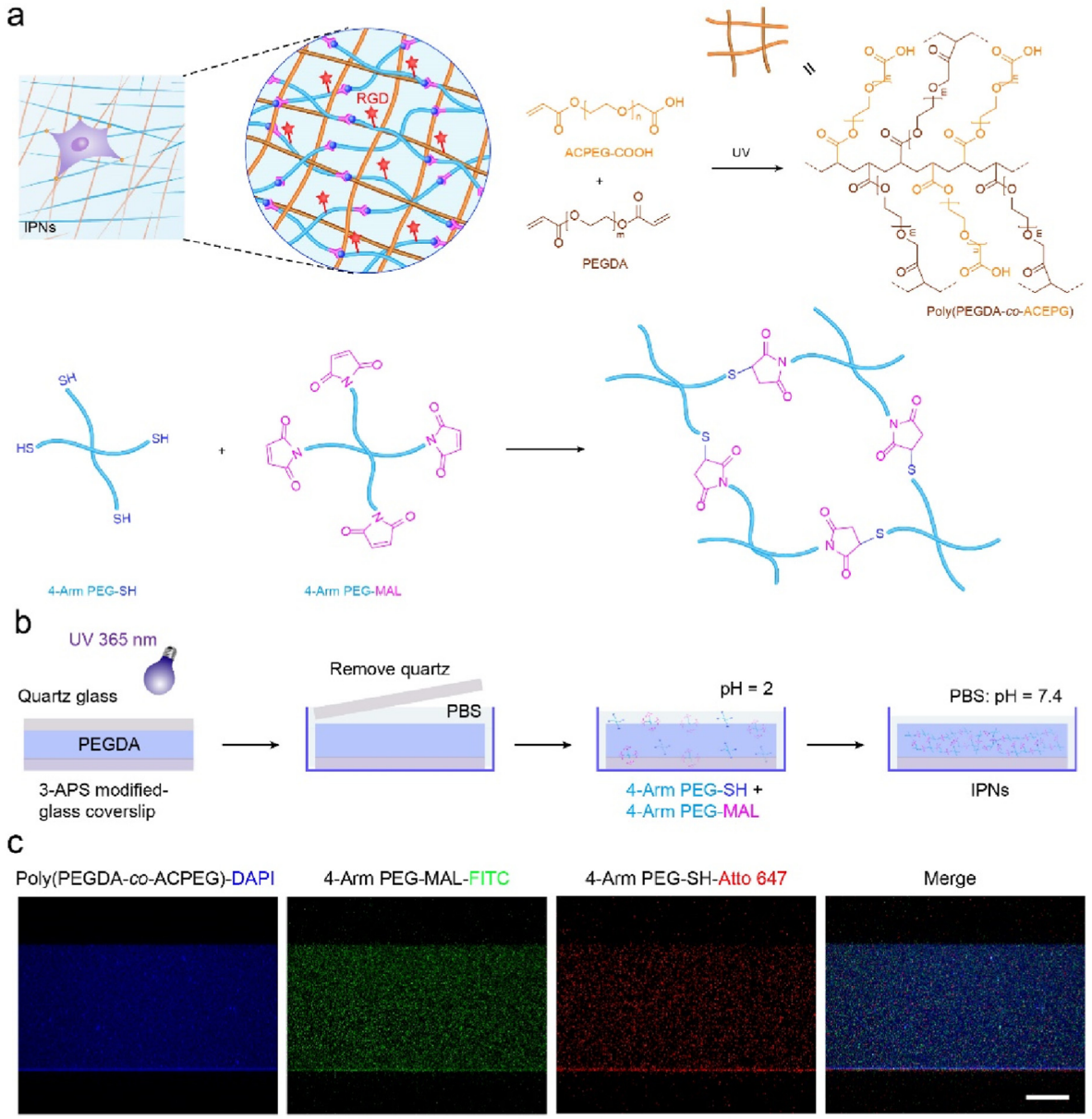

Fig. 1. a) Schematic view of the interpenetrating network of PEGDA host and 4-arm PEG guest with RGD ligands linked to the guest network. b) Procedure for the synthesis of the IPN: the poly (PEGDA-*co*-ACPEG) host gel is polymerized between two glass slides, one of them is functionalized with acrylate groups. After photoinitiated radical polymerization, the quartz cover is removed and the hydrogel is incubated with a solution of 4-arm PEG monomers at pH 2. After 2 h incubation, in which the guest 4-arm PEG chains diffuse into the PEGDA host, the guest network is crosslinked by changing the pH to 7.4. c) Scanning laser fluorescence images of a cross-section of the IPN hydrogel film after incubation with fluorescently labeled 4-arm PEGs. The images show that the components of the guest 4-arm PEG network are homogeneously distributed in the PEGDA host network. Scale bar: 50 μm. The film thickness is about 140 μm, see Table 1.

Table 1
Macroscopic properties of the host PEGDA SN and the IPN. The thickness of the wet gel was determined by confocal microscopy. The swelling ratio was determined by the weighting of the dry and wet gels. Young's modulus was determined by the indentation with an AFM colloidal probe. The shear storage and loss modulus were measured by rheology at frequencies between 0.01 and 1 Hz (Figure S4).

	Thickness-wet (μm)	Swelling ratio (by weight)	Shear Storage modulus (kPa)	Shear Loss modulus (Pa)	Young's modulus (kPa)-AFM indentation
SN	140.0 ± 6.4	12.5 ± 1.9	15.7 ± 0.9	11.6 ± 1.2	42.0 ± 3.5
IPNs	135.6 ± 6.7	14.0 ± 1.0	15.2 ± 0.1	11.4 ± 1.8	41.3 ± 4.0

In order to incorporate the guest network (Fig. 1b), the PEGDA hydrogel was incubated in a 2.5 *wt*% solution of 4-arm PEG-MAL (maleimide) and 4-arm PEG-SH (thiol) in citric acid buffer at pH 2. At this pH, the reaction between SH and MAL is not favored (Figure S5b in SI). The saturation concentration of the 4-arm PEGs into the PEGDA/COOH hydrogel was reached within 1-h incubation, as confirmed by fluorescence microscopy using fluorescently labeled 4-arm PEG-derivatives (Figure S2). The fluorescence image (Fig. 1c) indicates a homogeneous distribution of both precursors across the whole gel thickness, and evidences that the mesh size of the PEGDA network (expected mesh size 5.7 nm according to literature reports [12]) was large enough for the 4-arm PEG macromers to penetrate it. Crosslinking of 4-arm PEG-MAL and 4-arm PEG-SH was triggered by exchanging the citric buffer solution by PBS at pH = 7.4. At this pH, the crosslinking reaction between thiol and maleimide groups occurs within seconds (Figure S5a). The 4-arm PEGs chains are expected to intercalate within the PEGDA/COOH host hydrogel, but no covalent reaction between maleimide or thiol with COOH groups is expected. No inhomogeneity or phase separation was observed within the IPNs by confocal microscopy (Fig. 1c). The incorporation of the second network did not cause significant changes in the thickness or swelling ratio of the hydrogel (Table 1).

The mechanical properties of the hydrogels were evaluated by shear rheology and by indentation with an AFM colloidal probe, addressing millimeter and micrometer length scales. The PEGDA-*co*-ACPEG-COOH host gel exhibited an average Young's Modulus of 42 kPa, in indentations recorded across the hydrogel surface, indicating that the gel surface was homogeneous. The Young's Modulus of the IPN was similar to the PEGDA/COOH single network (Table 1). The shear storage and loss moduli were obtained by rheology. Similar values were observed for the IPN and the PEGDA/COOH SN. Predominantly elastic response was confirmed by the absence of a rate dependence for storage and loss modulus between 0.01 and 1 Hz (Figure S4). The SN and the IPN seem to be homogeneous and share similar mechanical properties at the macroscopic length scale in spite of having different network structures at the molecular scale.

In order to probe the nanomechanical response of the SN and the IPN, we performed single-molecule force spectroscopy experiments at the hydrogel surfaces with an atomic force microscope (AFM) (Fig. 2a). We were interested in differences in the molecular-scale stiffness between the two networks: the host PEGDA and the interpenetrating 4-arm PEG network. For this purpose, we selectively functionalized the polymer chains of either of the two networks with biotin (see experimental details in SI), and the AFM tip with streptavidin. The experimental procedure of single-molecule force spectroscopy on hydrogels and results for single PEGDA networks have been previously reported [12]. In short, the tip

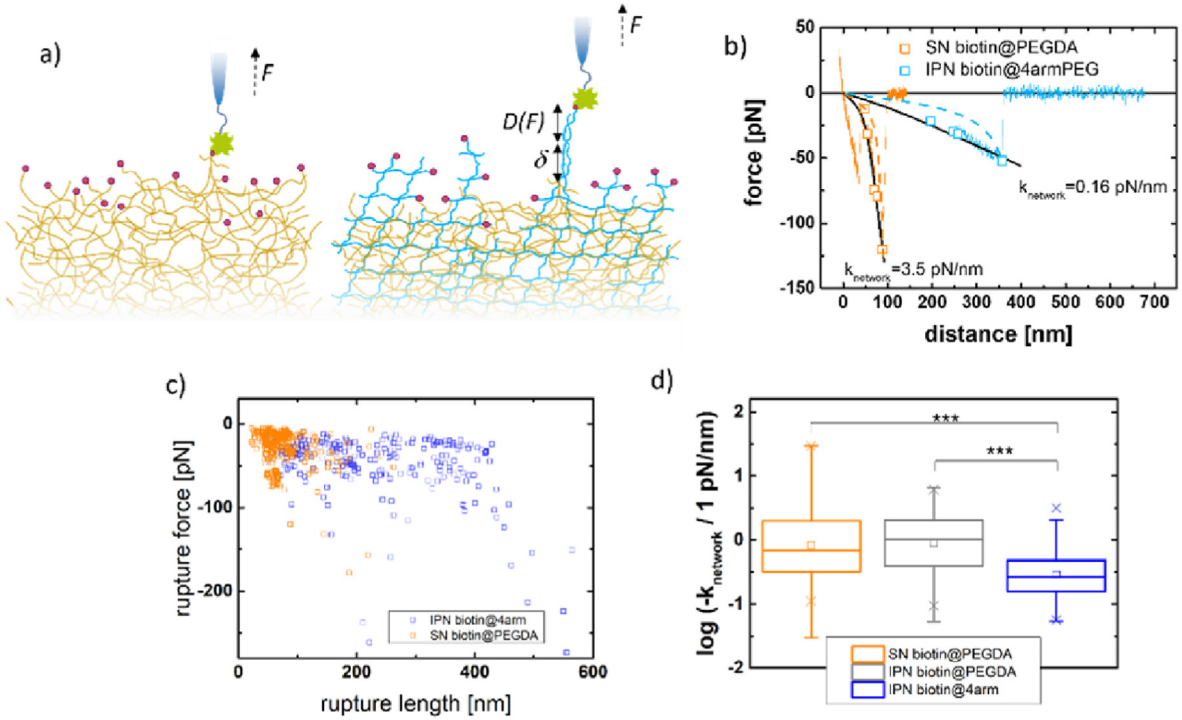

Fig. 2. a) Visualization of the nanomechanical characterization by single-molecule force spectroscopy. The PEGDA host network is represented by orange lines, the interpenetrating 4-arm PEG network by blue lines. One network is functionalized by biotin (red dots) and its stiffness at the single-linker level is probed by an AFM tip functionalized with streptavidin (green square with four binding sites). b) Example force-distance curves from single-molecule force spectroscopy. The square dots indicate the rupture force and rupture length of other forces curves recorded immediately before or after the example curves. Their coincidence with the respective example curve indicates that the same linker was probed repeatedly but that the biotin-streptavidin bonds broke at different forces. For comparison, model curves for single-PEG extension are shown as dashed lines and model curves including network compliance as solid black lines (see text). c) Rupture force and length for the unbinding of streptavidin at the AFM tip from biotin attached to linkers either to the PEGDA SN or to the 4-arm PEG network in the IPN. d) Boxplots report the distribution of values for the logarithm of the effective stiffness of single crosslinks $k_{network}$. The boxes indicate the 1st and 3rd quartile of the value distribution, the horizontal line indicates the median value.

was retracted from contact with the hydrogel surface, and a force-distance curve $F(D)$ was recorded. We analyzed the tip-sample distance and the force at the moment when the last biotin-streptavidin bond ruptured. Two exemplary force-distance curves are presented in Fig. 2b, one for the PEGDA single network and one for the 4-arm PEG network in the IPN. When pulling on the PEGDA network, the biotin-streptavidin ruptured at a distance of 90 nm and a force of 125 pN. For the 4-arm PEG network, the rupture occurred at a distance of 350 nm and a force of 50 pN.

Rupture forces and rupture distances for all force curves are provided in Fig. 2c, both for the PEGDA SN and the 4-arm PEG network in the IPN. The randomness of the hydrogel network and the statistical nature of the bond breaking lead to a wide distribution of values. To demonstrate differences between networks, we show and analyze the full distributions of force curves recorded on different networks and gels. Significant differences in the characteristic rupture length and in the rupture forces between the two networks are evident. Force curves recorded on the PEGDA network ruptured at shorter distances than force curves recorded on the interpenetrating 4-arm PEG network. The mean rupture length is three times larger in the IPN (227 nm) than in the SN (73 nm) and the mean rupture force is higher in IPN (−47 pN) than in the SN (−28 pN, Figure S12). The difference demonstrates that the nanomechanical properties of an interpenetrating network can be addressed separately by single-molecule force spectroscopy and that, at the molecular length scale, host and guest networks exhibit clear differences in their molecular mechanical properties. As summarized in the introduction, recent studies have parameterized and quantified rupture forces and tether lengths independently, and investigated their respective role as nanomechanical cues in cell adhesion [7–9,11] and differentiation [6]. Our study of nanomechanical cues delivered by an IPN as compared to its host network reveals differences in rupture force and rupture length. In the following, we argue that the effective crosslink stiffness can serve as description of the nanomechanical differences presented by IPN and SN.

For an interpretation of the AFM results, we will connect the measured values of rupture force and rupture length to the mechanical properties of the networks at the molecular scale. Toward this goal, we first discuss the characteristic shape of force-distance curves and then discuss the statistical distribution of rupture forces and lengths along these curves.

The measured force-distance curves $D(F)$ shown in Fig. 2b do not match the expected force-extension curves for single PEG polymers: The measured stiffness at the point of rupture is always significantly lower than the slope of a calculated force-extension curve at the same extension and the same force (dashed lines in Fig. 2b, for the calculation, see SI). This deviation is expected. The force applied to the linker leads to a displacement δ of its crosslinking point at the hydrogel surface. This crosslink serves as an anchor for the linker that is pulled on and is itself coupled to the random network by a small number of extensible polymers. The measured distance in force spectroscopy is the sum of the extension of the linker L_{PEG} and the displacement δ of the crosslinking point:

$$D(F) = L_{PEG}(N_{EG}, F) + \delta(F) \tag{1}$$

For a better model of the curves in Fig. 2b, we chose to combine the extension of a single PEG polymer ($N_{EG} = 182$) with a displacement of the network crosslink which is modeled as a linear spring with a spring constant $k_{network}$:

$$\delta = F/k_{network} \tag{2}$$

The choice of the linker length N_{EG} is motivated by the mean number of repeating units in one PEGDA monomer. Although the choice of one effective linker length and the assumption of linearity for the spring representing the network are simplifications of the mechanical response of the random network, there is a good agreement for all force-distance curves as exemplified by the solid black curves in Fig. 2b.

The two experimental force-distance curves provided in Fig. 2b with their specific rupture force and distance are examples. Rupture force and rupture distance can be lower or higher for the same linker, as the unbinding of the biotin-streptavidin bond is a statistical process [13,14]. The statistical distribution of rupture forces and of corresponding distances along each force-distance curve for a given linker is demonstrated by the additional data points for rupture events in Fig. 2b. The force curves represented by these data points have been recorded within minutes on the same spot of each surface. Comparison with force-distance curves confirms that the wide distribution of rupture forces represents the same linker for each series of data points.

We are not interested in the statistical distribution of rupture forces for the biotin-streptavidin bond, but in the mechanical properties of the hydrogel networks at the level of single polymeric linkers. For all data points on each force curve in Fig. 2b, the same parameter $k_{network}$ for the nanomechanical response should be reported since the same linker is probed. A single-parameter model which fits the data points in Fig. 2b well is the combination of linker extension and crosslink displacement introduced in Eqs. (1) and (2). The model results have been added to the plots as solid black lines, using different values for the network stiffness $k_{network}$.

We can now calculate the effective stiffness of single crosslinks for all data points presented in Fig. 2c. For each pair of rupture force F_{rup} and rupture length D_{rup}, the effective crosslink stiffness $k_{network}$ can be determined by the following calculation:

$$\delta_{rup} = D_{rup} - L_{PEG}(N_{EG},\ F_{rup}) \tag{3}$$

$$k_{network} = F_{rup}/\delta_{rup} \tag{4}$$

The resulting range of values for the effective stiffness of crosslinks in the two networks is presented in Fig. 2d, using the parameter $N_{EG} = 182$ as discussed above. The analysis quantifies the observed difference in molecular-scale stiffness between the PEGDA host network and the interpenetrating 4-arm PEG guest network. For the former, the stiffness of single crosslinks against displacement ranges from 0.3 to 1.9 pN/nm (1st and 3rd quartile), while for the latter values range from 0.16 to 0.48 pN/nm, with median values of 0.64 and 0.26 pN/nm. The median values must be interpreted with care in the description of networks, because they depend on how often each linker was probed. This number varies greatly between linkers. We have not yet found a reliable criterium to identify groups of force curves recorded on the same linker. However, the range of stiffness values for each network is correctly displayed by the boxplots.

Single-molecule force spectroscopy is equally suitable to probe the molecular mechanics of the PEGDA host network after the addition of the 4-arm PEG guest network and thus can separately quantify the molecular stiffness of two interpenetrating networks. As expected, the range of molecular stiffness values is similar for the PEDGA single network and for the PEGDA host network in the IPN (Fig. 2d). A fully crosslinked 4-arm PEG network can be expected to have a comparable or higher stiffness on the molecular scale than a crosslinked PEGDA network. The centers of connected 4-arm PEG molecules are connected by polymers with 108 repeating units and they constitute crosslinks with a fixed connectivity of 4. PEGDA networks are built by polymers of 182 repeating units between crosslinks with a varying connectivity probably smaller than 4. The lower molecular stiffness observed in our experiment indicates that the interpenetrating 4-arm PEG network, which was formed within the existing PEGDA network matrix, was not fully crosslinked.

In summary, the SN and IPN hydrogels studied in our experiments present the same macroscopic Young's Modulus independent of the presence of the interpenetrating 4-arm PEG, while single-molecular force spectroscopy revealed that the average stiffness of the two networks on the molecular scale is very different.

We used the developed hydrogels to study cellular adhesion in the different mechanical scenarios, i.e. mediated by either the single PEGDA

network or the interpenetrating 4-arm PEG network. For the functionalization of the hydrogels, we coupled RGD peptides using the same linkers as in the biotin functionalization in single-molecule force spectroscopy. A RGDfK sequence was used to modify the COOH groups of the PEGDA/COOH SN, and a RGDfC was used to functionalize the 4-arm PEG network in the IPN (Fig. 3a, see Methods for details in SI). Functionalization conditions were optimized to achieve comparable RGD density on both gels (Figure S7-8). Fibroblasts (L929) seeded on the hydrogels attached and spread well on the RGDfK modified SN and on the RGDfC modified IPN. The spreading area quantified after 24 h were found similar for the SN and the IPN (Fig. 3c), although the adhesion was mediated by the PEGDA network in one case and by the 4-arm PEG

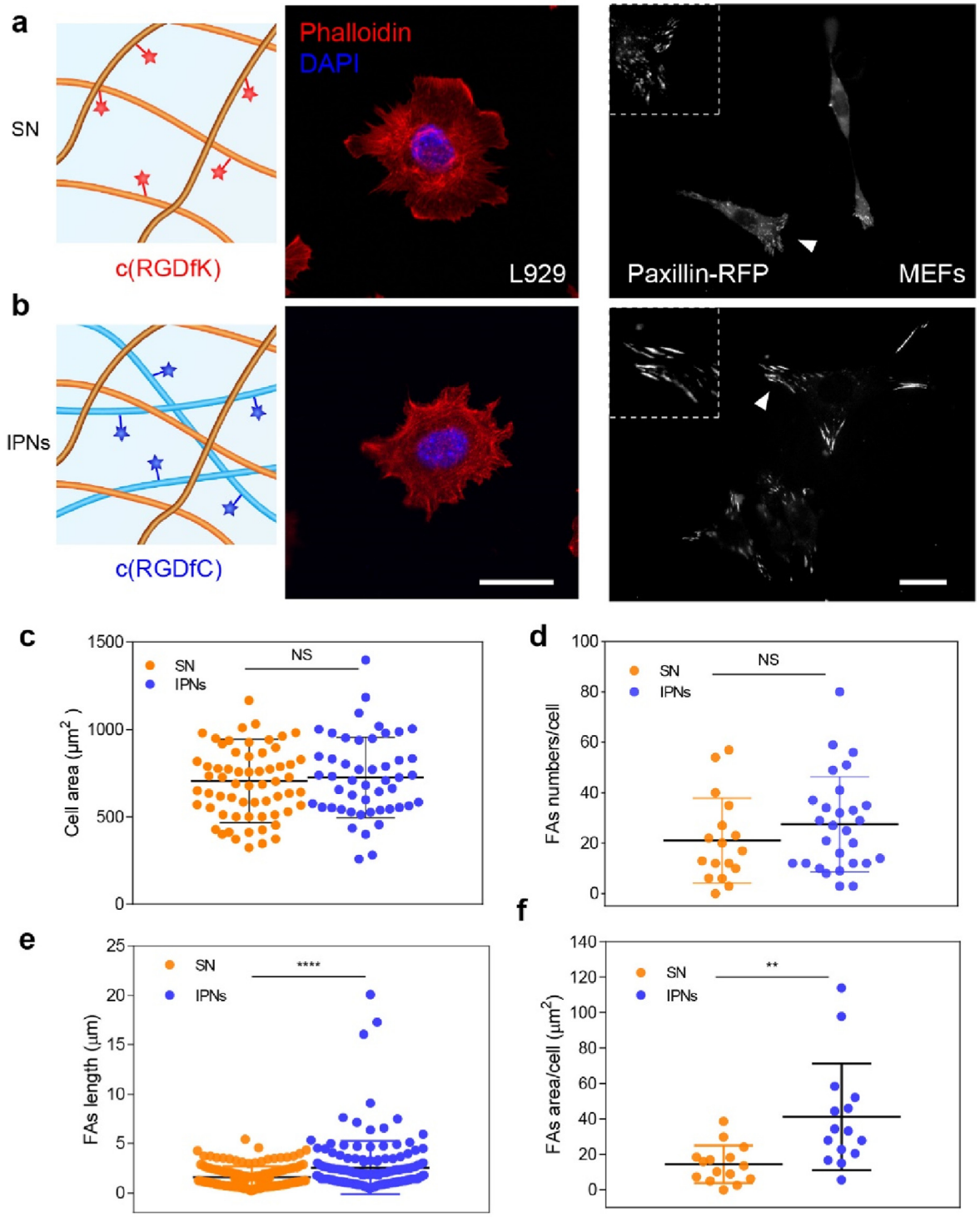

Fig. 3. a). a-b) Attachment and spreading of fibroblast cells (L929 or MEFs) on SN and IPN hydrogels after 24 h seeding. Hydrogels are functionalized with RGDfK and RGDfC, respectively. L929 cells were stained with phalloidin (red) and DAPI (blue) to image F-actin and the nucleus. MEF cells transfected with the paxillin-RFP mutants were used for focal adhesion study. Scale bars 25 μm. c) Average area per L929 cell measured on SN and IPN. d) Number of focal adhesions per MEF cell. e) Area in focal adhesions per MEF cell. f) Length of focal adhesions. Mean ± s.d, "ns" indicates no statistical difference, ** $p < 0.01$, **** $p < 0.0001$, as calculated by non-parametric T-tests.

network in the other case.

We also investigated cell adhesion on an IPN where the PEGDA host network was functionalized by RGDfK while the guest 4-arm PEG network was not functionalized. In this case, we observed a low number of attached fibroblasts and weak spreading. Note that the SN and the IPN presented the same RGD density (Figure S8). We suggest that the loose arms of the interpenetrating 4-arm PEG network on the top of the IPN hydrogel hamper the access of the membrane receptors to the RGDfK binding motifs at the ACPEG linkers. The attachment of the cells to the PEGDA network within the IPN is then hindered, similar to the known reduction of cell adhesion by PEG brushes on surfaces [15,16]. Note that this hindrance was not observed with the AFM probe and the biotin modified IPN in the single-molecule force spectroscopy experiment.

We also investigated single networks of 4armPEG, functionalized with biotin for AFM force spectroscopy and with RGDfC for cell adhesion experiments. The results were omitted from the discussion in this study because they could not be compared with SN PEGDA and IPN results. In AFM force spectroscopy, most force curves indicated the rupture of multiple biotin-streptavidin bonds, probably due to a high density of biotin binding sites on the SN 4-arm PEG network. In cell experiments, we observed attachment but no quantifiable cell spreading, probably due to the low elastic modulus of only 13 kPa.To summarize the cell area results in Fig. 3c), we observed that similar macroscopic mechanical properties of gels in combination with similar RGD density lead to a comparable cell attachment and spreading behavior of L929 fibroblasts on the RGDfK/PEGDA single network and on the RGDfC/4-arm PEG network interpenetrating the PEGDA host network.

Mechanosensing by cells involves the clustering of receptor/ligand complexes to form focal adhesions (FAs) [17–19]. Cells sense and respond to the mechanical properties of the extracellular matrix (or biomaterial) by the reorganization of their stress fibers and adjusting contractility [2,20,21]. This adjustment influences the geometry of the focal adhesions. To understand if the nanomechanical responses of the hydrogels affect FAs, mouse embryo fibroblasts (MEFs) expressing paxillin-RFP were cultured on the hydrogels. Optical microscopy of the paxillin-RFP reveals the number and shape of the focal adhesion complexes (Fig. 4a). The number, length, and area of FAs were quantified after cell seeding for 24 h. Focal adhesions were significantly larger and longer on IPNs with RGDfC on 4-arm PEG linkers than on SN with RGDfK on ACPEG linkers. On PEGDA networks, about 10 FAs were found in a single cell and the average FA area and length were 14 μm^2 and 1.6 μm. On interpenetrating 4-arm PEG networks, we observed about 18 FAs per cell, with an average FA area and length of 40 μm^2 and 2.6 μm. We suggest that the larger size of FAs on the IPNs originated from the difference in nanometer-scale mechanical properties. In the IPNs, the RGD ligands are attached to the 4-arm PEG network which exhibits a significantly lower stiffness of single crosslinks. The flexibility of the linkers can facilitate clustering of the ligands and result in an effective increase of the local RGD ligand density and increased FA areas. In recent work, Attwood and coworkers have shown that the RGD tether length has a strong effect on the size and length of focal adhesions, as well as on cell spreading and attachment independent of matrix mechanics [8]. Our results corroborate their findings in hydrogels with different architectural design. To further compare our results with those of Attwood et al. the median extension of our hydrogel-anchored linkers under the integrin-activating force of 43 pN is 114 nm for the SN and 212 nm for the IPN. For these effectively longer linkers they reported a significant reduction in the density of cells on the surface and in the cell area.

In order to confirm the influence of nanomechanical stimuli on the biochemical pathways of adhesion regulation, we studied the local distribution of the YAP protein in cells adhering to SNs or IPNs. The ability of cells to spread and to perceive the extracellular mechanics is associated to the Hippo pathway effector Yes-associated protein (YAP), which acts as an 'on-off' mechanosensitive transcriptional regulator [22,23]. Both biochemical and mechanical cues control YAP's main regulatory mechanism, namely its localization in either the cytoplasm or the nucleus. A number of studies have suggested that stiffer substrates activate YAP by dephosphorylation, and YAP translocates from the cytoplasm to the nucleus [24,25]. With recent evidence suggesting an interplay between FAs and nuclear YAP [26,27], we investigated YAP nuclear localization in L929 fibroblasts cultured on the PEGDA/RGDfK single network and on the 4-arm PEG/RGDfC interpenetrating network (Fig. 4a, Figure S12). We sought to study whether YAP nuclear accumulation correlated with the FA size and, therefore, with the nanometer-scale mechanics of these networks.

The ratio of nuclear to cytoplasmic YAP for the 4-arm PEG/RGDfC IPN is double of the one for PEGDA/RDGfK SN hydrogels (Fig. 4b). YAP levels on 4-arm PEG/RGDfC IPN hydrogels were significantly higher than on the PEGDA/RGDfK single network. These trends correlate with the results for FA area and length and with the difference in nanomechanical response, but not with results from the cell spreading area, where no differences were observed between the single and interpenetrating network hydrogels.

It is well accepted that cells show an increased integrin mechanotranduction response (and downstream YAP activation) on hydrogels with a higher bulk stiffness compared to lower stiffness. Through single force spectroscopy studies we show that the effective stiffness at the molecular scale for the IPN is lower than for the SN, while the bulk stiffness is the same. In contrast to our initial predictions, cells showed a higher integrin activation and YAP nuclear translocation on the "softer" IPN, than on the "stiffer" SN. These results suggest that cells may sense something other than the bulk stiffness. This is in line with other studies that show that factors such as ligand spacing [28], ligand mobility [29,30], tether length [8] and surface roughness [31] can influence integrin

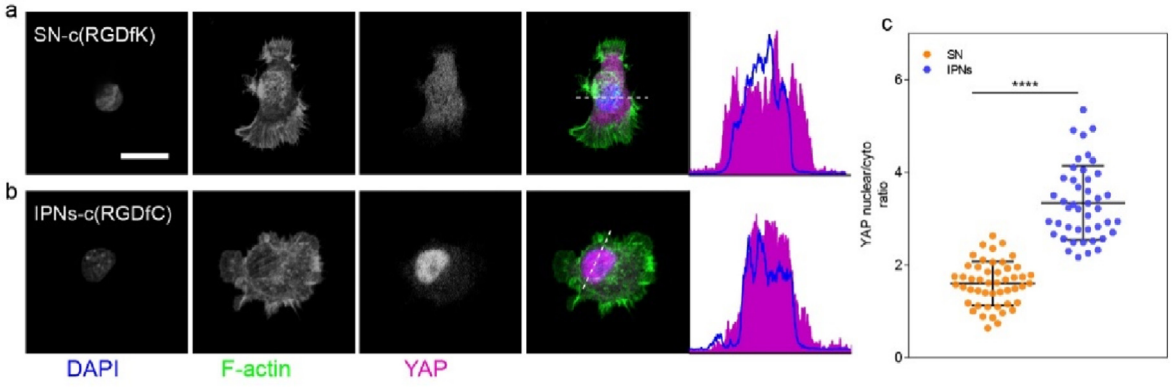

Fig. 4. Fluorescence microscopy of the local distribution of the YAP protein in L929 cells spreading on SN (a) and IPN hydrogels (b). Cells were stained with Phalloidin (green) for F-actin visualization, with anti-YAP (magenta), and nuclei were stained DAPI (blue), scale bar 25 um. c) Quantification of the ratio of YAP in nucleus and cytoplasm based on stacks of fluorescence images like the ones shown in figure a and b. Mean ± s.d, ****$p < 0.0001$, as calculated by non-parametric T-tests.

mechanotransduction. The cell response in integrin activation due to bulk substrate rigidity seems to be biphasic and is dependent on ligand spacing [28]. As ligand spacing increases, the optimal rigidity for integrin activation and subsequent collapse decreases. By switching from our SN-attached RGD adhesion to the IPN-attached adhesion sites, we may effectively decrease local ligand spacing due to longer ligand tethers. This may explain why we see higher integrin activation and downstream YAP translocation on the IPN network than on the SN, while keeping bulk stiffness constant. In contrast, Atwood et al. found higher integrin activation with shorter RGD-tethers compared to their longer tethers [8]. This discrepancy may be explained by their use of very stiff glass substrates, compared to our medium-stiff hydrogel system. Alternatively, due to technical differences in AFM measurements, the length scales of our experiments do not match up. The increased tether length of the IPN may also be thought of as having a higher ligand mobility, which also has been shown to promote cell adhesion [29].

In conclusion, interpenetrating networks of PEGDA and 4-arm PEG offer different mechanical stiffness at the scale of single crosslinks. Single-molecule force spectroscopy studies revealed a lower stiffness of the interpenetrating, less dense network at the level of single linkers compared to the single, denser, host network. Our data suggest that cells attached to the "soft" linkers of the IPN behaved as if they were adhering to an IPN with higher ligand concentration. This result is in agreement with recent work by Charrier [11]. Our findings also support the statement that the regulation of the Hippo pathway is under the control of focal adhesions [32]. The feedback from the local stiffness of the IPNs hydrogels likely has important implications for the molecular processes leading to the assembly of focal adhesions. Our results demonstrate the inherent capability of interpenetrating network designs to provide very different mechanical signals at the molecular scale just by combining networks of different topology and connectivity, while maintaining the overall macroscopic response. These materials can help to identify and reconstruct local and macroscopic features that guide cell response to synthetic and natural materials.

Credit author statement

Bin Li, **Roland Bennewitz**, **Aránzazu del Campo**, Conceptualization; **Bin Li**, **Arzu Çolak**, **Johanna Blass**, **Jingnan Zhang**, **Yijun Zheng**, **Qiyang Jiang**: Investigation; **Bin Li, Arzu Çolak, Roland Bennewitz**: Methodology; **Bin Li, Mitchell Han**, **Roland Bennewitz**, **Aránzazu del Campo**: Writing - Review & Editing; **Bin Li, Mitchell Han**, **Roland Bennewitz**: Formal analysis; **Bin Li, Arzu Çolak, Roland Bennewitz**: Visualization; **Roland Bennewitz, Aránzazu del Campo**: Supervision; **Bin Li, Roland Bennewitz, Aránzazu del Campo**: Funding acquisition.**Dr. B. Li, Dr. A. Çolak, Dr. J. Blass, Dr. J. Zhang**, **Dr. Y. Zheng, Q. Jiang**, **Dr. M. Han**, **Prof. R. Bennewitz**, **Prof. A. del** CampoINM–Leibniz Institute for New Materials Campus D2 2, 66,123 Saarbrücken, Germany E-mail: bin1.li@tum.de; roland.bennewitz@leibniz-inm.de; aranzazu.delcampo@leibniz-inm.de; Prof. A. del Campo Chemistry Department, Saarland University 66,123 Saarbrücken, Germany; **Prof. R. Bennewitz** Physics Department, Saarland University 66,123 Saarbrücken, Germany.

Data availability

The data that support the findings of this study are available from the corresponding author upon reasonable request.

Declaration of competing interest

The authors declare that they have no known competing financial interests or personal relationships that could have appeared to influence the work reported in this paper.

Acknowledgements

Bin Li gratefully acknowledges fellowship support by the Alexander von Humboldt Foundation. M. Han, J. Zhang, Y. Zheng, and A. del Campo acknowledge the financial support from DFG (SFB1027). The authors thank Dr. Michael Kappl and Dr. Regina Fuchs at MPIP for help with the preparation of AFM colloidal probes and helpful discussions.

Appendix A. Supplementary data

Supplementary data to this article can be found online at https://doi.org/10.1016/j.mtbio.2022.100323.

References

[1] J.R. Garcia, A.J. Garcia, Nat. Mater. 13 (2014) 539.
[2] J.T. Parsons, A.R. Horwitz, M.A. Schwartz, Nat. Rev. Mol. Cell Biol. 11 (2010) 633.
[3] W.L. Murphy, T.C. McDevitt, A.J. Engler, Nat. Mater. 13 (2014) 547.
[4] A.D. Celiz, J.G. Smith, R. Langer, D.G. Anderson, D.A. Winkler, D.A. Barrett, M.C. Davies, L.E. Young, C. Denning, M.R. Alexander, Nat. Mater. 13 (2014) 570.
[5] F.M. Watt, W.T. Huck, Nat. Rev. Mol. Cell Biol. 14 (2013) 467.
[6] J.H. Wen, L.G. Vincent, A. Fuhrmann, Y.S. Choi, K.C. Hribar, H. Taylor-Weiner, S. Chen, A.J. Engler, Nat. Mater. 13 (2014) 979.
[7] E. Battista, F. Causa, V. Lettera, V. Panzetta, D. Guarnieri, S. Fusco, F. Gentile, P.A. Netti, Biomaterials 45 (2015) 72.
[8] S.J. Attwood, E. Cortes, A.W. Haining, B. Robinson, D. Li, J. Gautrot, A. Del Rio Hernandez, Sci. Rep. 6 (2016), 34334.
[9] D. Kong, W. Megone, K.D.Q. Nguyen, S. Di Cio, M. Ramstedt, J.E. Gautrot, Nano Lett. 18 (2018) 1946.
[10] C. Matellan, A.E. Del Rio Hernandez, J. Cell Sci. 132 (2019) jcs229013.
[11] E.E. Charrier, K. Pogoda, R.G. Wells, P.A. Janmey, Nat. Commun. 9 (2018) 449.
[12] A. Colak, B. Li, J. Blass, K. Koynov, A. Del Campo, R. Bennewitz, Nanoscale 11 (2019), 11596.
[13] C. Friedsam, A. KWehle, F. Kühner, H.E. Gaub, J. Phys. Condens. Matter 15 (2003) S1709.
[14] E. Evans, Annu. Rev. Biophys. Biomol. Struct. 30 (2001) 105.
[15] H. Du, P. Chandaroy, S.W. Hui, Biochim. Biophys. Acta, Biomembr. 1326 (1997) 236.
[16] Y.J. Oh, E.S. Khan, A.D. Campo, P. Hinterdorfer, B. Li, ACS Appl. Mater. Interfaces 11 (2019), 29312.
[17] B. Geiger, J.P. Spatz, A.D. Bershadsky, Nat. Rev. Mol. Cell Biol. 10 (2009) 21.
[18] R. J. P. Jr., Y.-l. Wang, Proc. Natl. Acad. Sci. USA 94 (1997), 13661.
[19] K. Burridge, M. Chrzanowska-Wodnicka, Annu. Rev. Cell Dev. Biol. 12 (1996) 463.
[20] M.A. Schwartz, Cold Spring Harbor Perspect. Biol. 2 (2010) a005066.
[21] J. Fu, Y.-K. Wang, M.T. Yang, R.A. Desai, X. Yu, Z. Liu, C.S. Chen, Nat. Methods 7 (2010) 733.
[22] J.M. Lamar, P. Stern, H. Liu, J.W. Schindler, Z.G. Jiang, R.O. Hynes, Proc. Natl. Acad. Sci. U.S.A. 109 (2012) E2441.
[23] A. Nukuda, C. Sasaki, S. Ishihara, T. Mizutani, K. Nakamura, T. Ayabe, K. Kawabata, H. Haga, Oncogenesis 4 (2015) e165.
[24] S. Dupont, L. Morsut, M. Aragona, E. Enzo, S. Giulitti, M. Cordenonsi, F. Zanconato, J. Le Digabel, M. Forcato, S. Bicciato, N. Elvassore, S. Piccolo, Nature 474 (2011) 179.
[25] A. Elosegui-Artola, I. Andreu, A.E.M. Beedle, A. Lezamiz, M. Uroz, A.J. Kosmalska, R. Oria, J.Z. Kechagia, P. Rico-Lastres, A.L. Le Roux, C.M. Shanahan, X. Trepat, D. Navajas, S. Garcia-Manyes, P. Roca-Cusachs, Cell 171 (2017) 1397.
[26] V.K. Raghunathan, J.T. Morgan, B. Dreier, C.M. Reilly, S.M. Thomasy, J.A. Wood, I. Ly, B.C. Tuyen, M. Hughbanks, C.J. Murphy, P. Russell, Invest. Ophthalmol. Vis. Sci. 54 (2013) 378.
[27] G. Halder, S. Dupont, S. Piccolo, Nat. Rev. Mol. Cell Biol. 13 (2012) 591.
[28] R. Oria, T. Wiegand, J. Escribano, A. Elosegui-Artola, J.J. Uriarte, C. Moreno-Pulido, I. Platzman, P. Delcanale, L. Albertazzi, D. Navajas, X. Trepat, J.M. Garcia-Aznar, E.A. Cavalcanti-Adam, P. Roca-Cusachs, Nature 552 (2017) 219.
[29] L. Yu, Y. Hou, W. Xie, J.L.C. Camacho, C. Cheng, A. Holle, J. Young, B. Trappmann, W. Zhao, M.F. Melzig, E.A. Cavalcanti-Adam, C. Zhao, J.P. Spatz, Q. Wei, R. Haag, Adv. Mater. 32 (2020), 2002566.
[30] L. Yu, Y. Hou, W. Xie, J.L. Cuellar-Camacho, Q. Wei, R. Haag, Adv. Mater. 32 (2020), 2006986.
[31] Y. Hou, L. Yu, W. Xie, L.C. Camacho, M. Zhang, Z. Chu, Q. Wei, R. Haag, Nano Lett. 20 (2020) 748.
[32] G. Nardone, J. Oliver-De La Cruz, J. Vrbsky, C. Martini, J. Pribyl, P. Skládal, M. Pešl, G. Caluori, S. Pagliari, F. Martino, Z. Maceckova, M. Hajduch, A. Sanz-Garcia, N.M. Pugno, G.B. Stokin, G. Forte, Nat. Commun. 8 (2017), 15321.